

Application of time–temperature superposition principle to Chinese fir orthotropic creep

Hui Peng^{1,2} · Jiali Jiang¹ · Jianxiong Lu¹ · Jinzhen Cao²

Received: 16 January 2017 / Accepted: 29 April 2017 / Published online: 3 June 2017
© The Japan Wood Research Society 2017

Abstract The application of time–temperature superposition principle (TTSP) to orthotropic creep in dry Chinese fir (*Cunninghamia lanceolata* [Lamb.] Hook.) was investigated through a sequence of short-term tensile creep for longitudinal (L), radial (R), and tangential (T) specimens in the temperature range of 30–150 °C. A visual assessment for the validity of TTSP was carried out by applying the approximated complex plane (ACP). The results showed that TTSP was well matched for R and T specimens using horizontal shift factor to construct master curves. As for L specimen, an additional vertical shift factor was applied to construct a smooth master curve, owing to the temperature-dependent compliance. Based on the application of ACP, the creep model governed by a power law was proposed to successfully depict the master curve for each main anatomy direction. The present study partially provided the firsthand data in verifying the applicability of TTSP of the orthotropic viscoelasticity of Chinese fir wood, and successfully constructed the rheological model to predict the orthotropic

creep response. More importantly, the result can function as the base to the structural safety designs for the engineering structures of Chinese fir in practice.

Keywords Chinese fir · Orthotropic creep · Time–temperature superposition principle · Power law model

Introduction

Wood, like most polymeric materials, exhibits a viscoelastic behavior depending on both temperature and the duration of the applied stress. The time-dependent behavior, such as creep and relaxation, of wood is of critical importance in engineering applications [1–4]. For this reason, it is desirable to investigate the viscoelastic behavior of wood over time scales that extend as long as the working life of wooden products. Unfortunately, practical considerations limit a lengthy creep or relaxation test, and an alternative approach to determine the time-dependent behavior of wood is to use the time–temperature superposition principle (TTSP) to obtain an extended range of time. The TTSP is based upon the theory that increasing the temperature is equivalent to stretching the real time of the viscoelastic response [5–9]. In this approach, viscoelastic properties can be determined by static measurements (e.g., creep or stress relaxation) or by dynamic measurements using frequency-multiplexing experiments over a wide range of temperatures. By selecting a reference curve at the desired temperature and shifting the data at other temperatures to the reference temperature (horizontal shifts on the log time or log frequency axis), a master curve is generated over several decades of time or frequency domain. The curve can be used to predict the long-term effects of stress/strain on wood properties.

✉ Jianxiong Lu
jianxiong@caf.ac.cn

✉ Jinzhen Cao
caoj@bjfu.edu.cn

Hui Peng
penghyx@126.com

Jiali Jiang
jjialiwood@caf.ac.cn

¹ State Key Laboratory of Tree Genetics and Breeding, Research Institute of Wood Industry, Chinese Academy of Forestry, Beijing 100091, People's Republic of China

² College of Materials Science and Technology, Beijing Forestry University, Beijing 100083, People's Republic of China

The empirical relationship between temperature and time effect of stress/strain on deformation and relaxation processes (i.e., the horizontal shift factor required to transpose the temperature effect to the corresponding time effect) is formulated in two well-known mathematical functions: William–Landel–Ferry (WLF) equation and Arrhenius law. The WLF equation, enunciated by Williams et al. [10], is given by Eq. (1), and the activation energy (ΔH) can also be expressed by WLF equation using Eq. (2):

$$\log a_T = -C_1(T - T_0)/[C_2 + (T - T_0)], \quad (1)$$

$$\Delta H = R \cdot d(\log a_T)/dT, \quad (2)$$

where a_T is the horizontal shift factor on the log time axis to transpose the creep or relaxation value at short time and higher temperature to the appropriate time scale expected at a lower temperature, T the measurement temperature, T_0 the reference temperature, C_1 and C_2 two WLF constants, and R the universal gas constant. The WLF equation describes the time–temperature stress/strain response behavior of a polymer at/near its glass transition temperature, which is suitable to be used for amorphous polymer systems. The Arrhenius law is usually used to relate the horizontal shift factor with respect to temperature and is given by

$$\log a_T = \Delta H/2.303R \cdot (1/T - 1/T_0), \quad (3)$$

where a_T is the horizontal shift factor, ΔH the activation energy, T the measurement temperature, T_0 the reference temperature, and R the universal gas constant. The Arrhenius law is typically used to determine the activation energy associated with the glass transition process.

Research has shown that TTSP was originally developed for amorphous polymers. However, wood is a composite biopolymer consisting of cellulose, hemicelluloses and lignin, and the time-dependent behavior of wood is determined by both oriented crystalline cellulose and

amorphous matrix made up of lignin and a variety of hemicelluloses. Given multiple transition regions from the thermorheological point, the TTSP's applicability to wood is sometimes controversial [8–15]. Macroscopically, wood is normally described as an anisotropic material with unique and independent mechanical behaviors in three mutually perpendicular directions: longitudinal direction, radial and tangential directions in the transverse plane [16–18]. In general, investigators study of TTSP's applicability to wood mainly focuses on the longitudinal or radial direction, but rarely provides a comprehensive dataset of TTSP's applicability among the three directions.

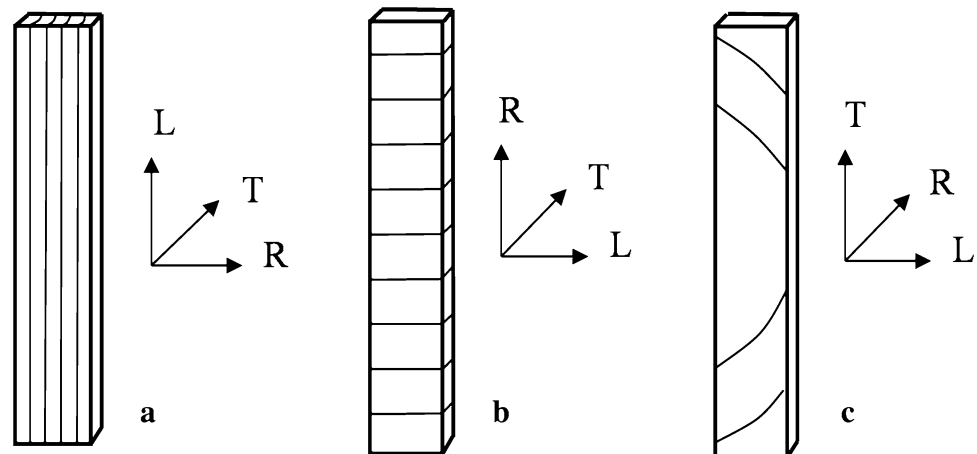
The objective of this study was to evaluate the applicability of TTSP in longitudinal, radial, and tangential directions for dry wood and observe the orthotropic creep using TTSP. Additionally, a generic creep model applicable in three main anatomy directions for dry wood was identified as well for obtaining the creep behavior over reasonable time periods.

Materials and methods

Wood material

Specimens for creep tests were cut successively within the same growth ring ranges and free of any visual defects in the heartwood part of Chinese fir (*Cunninghamia lanceolata* [Lamb.] Hook.) logs. Specimens with longitudinal (L), radial (R) and tangential (T) grain directions were prepared as shown in Fig. 1, and the dimension of the specimens was 35 mm × 6 mm × 1.5 mm. All the specimens were dried in a sealed container with anhydrous phosphorus pentoxide (P_2O_5) at room temperature until no weight loss was observed (not less than 2 weeks). The corresponding moisture content value and raw density of specimens were about 0.6% and 0.37 g/cm³, respectively.

Fig. 1 Specimens in three directions. **a** Longitudinal, **b** radial, and **c** tangential



Experimental methods

Creep behavior was performed on a dynamic mechanical analyzer (DMA 2980, TA Instruments) using a dry air purge of the sample chamber with tensile clamp, and a distance of 17 mm between clamping midpoints was used (Fig. 2). To make sure the specimen was straight, a pre-load force of 0.01 N was applied briefly. Subsequently, each specimen was subjected to isothermal creep segments for 20 min at each 10 °C interval in a temperature range of 30–150 °C, and 20 min equilibration/recovery periods were inserted between creep segments, as illustrated in Fig. 3.

The limit of linearity was determined using a stress–strain sweep, for which the L, R, and T specimens were deformed with increasing stress, respectively. Generally,

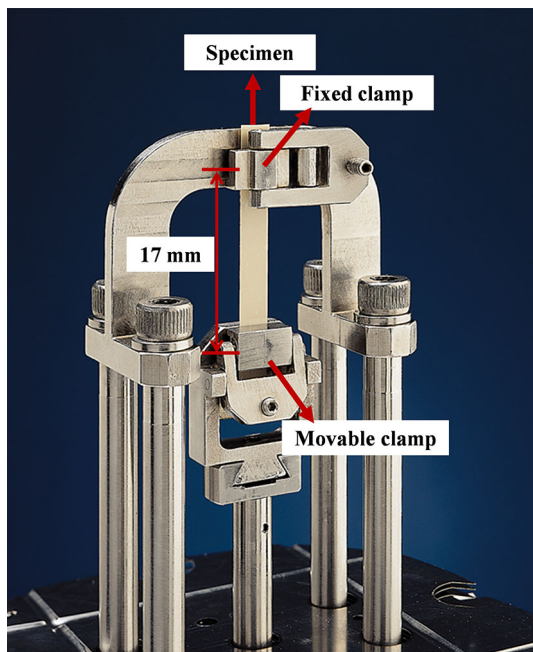


Fig. 2 Illustration of mounted sample ready for tensile mode of loading

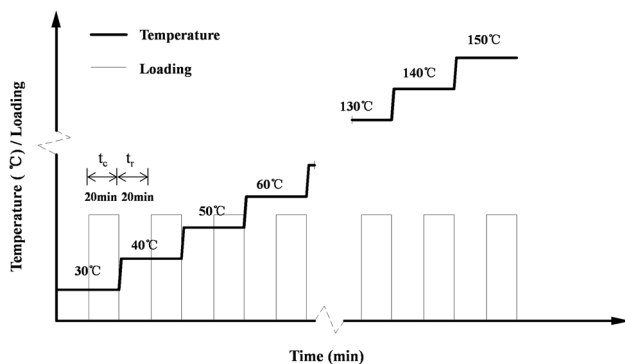


Fig. 3 Applied cycling schedule. t_c Creep time; t_r recovery time

wood behaved linearly up to 50% of the ultimate stress [2, 19]. Dried specimens were heated to the maximum experimental temperature 150 °C at 10 °C/min and held there for 10 min before the stress–strain sweep. The ultimate tensile stress of L specimen was not reached owing to the 2.1 MPa maximum stress of DMA 2980; therefore, the stress value of 1.3 MPa was selected. With regard to the R and T specimens, the stress level was set as 20% of ultimate tensile stress (2.0 MPa in R and 0.8 MPa in T), i.e., stress values were 0.40 MPa, and 0.16 MPa for the R and T specimens, respectively.

Data analysis

A representation relying on the use of the “approximated complex plane” (ACP), proposed by Dlouhá et al. [8], was used to analyze the creep data in this study. This method allowed the data from static tests to be represented in complex plot in the same way as a Cole–Cole graph using complex modulus (E' with respect to E'') for dynamic tests. According to Alfrey’s approximation [20], the storage compliance J' and loss compliance J'' components of complex compliance were applied for static test and can be written as:

$$J' \approx J(\log t), \tag{4}$$

$$J'' \approx \pi/2 \cdot dJ/d(\ln t) \approx \pi/2 \ln(10) \cdot dJ(\log t)/d \log t, \tag{5}$$

where t is the creep time and J the creep compliance.

The ACP is based on a visual assessment of the trajectories in the complex planes (J'' with respect to J'), which can be understood as a type of phase diagram presenting the slope against the value, relative to the function $J(\log t)$. The assumption of TTSP requires that individual creep curves induce one continuous curve in the ACP, as this would ensure that not only the values of the $J(\log t)$ functions match, but also the slope. Furthermore, the ACP is a convenient way to represent synthesized viscoelastic properties of wood [8].

Results and discussion

Building of the master curve using $\log t$ shifts

Short-term experimental data for increasing temperature levels were obtained, and a sequence of curves for L, R, and T specimens were plotted as compliance versus time with log scale (Fig. 4). The individual creep curves in the left panel of Fig. 4 represent the creep compliance changes over 20 min for 13 temperature levels (10 °C intervals in the range 30–150 °C). The curves showed the expected

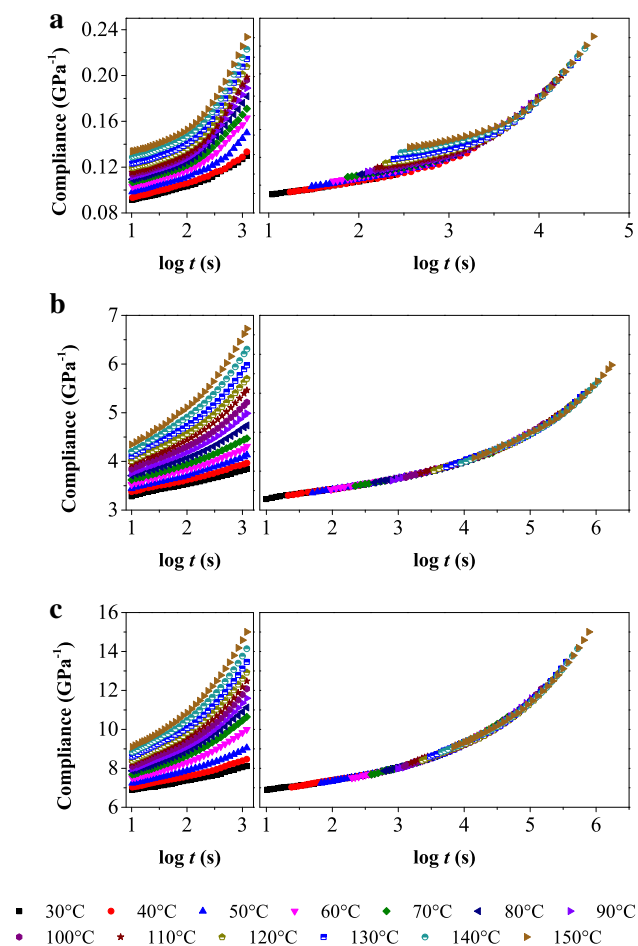


Fig. 4 (Right panel) Master curves obtained by shifting individual raw data curves (left panel) along $\log t$ for the L (a), R (b) and T (c) specimens. Curves measured at 30 °C are taken as a reference

response from isothermal creep segments: increasing creep compliance with time and temperature for each specimen irrespective of grain orientation [2, 7, 21]. There were differences in compliance among the specimens with three grain orientations. Compliance for L specimen was significantly lower than that for the R and T specimens, and the T specimen was higher than the R specimen almost twice. This result was consistent with previous studies [2, 14, 22]. The formation in anatomical structure could explain the differences of wood mechanical behavior among the L, R, and T specimens. Tracheids are strictly aligned in the L direction, which provide mechanical integrity to counteract load and influence the higher stiffness and lower compliance for the L specimen [23, 24]. For the transverse (R and T) specimens, some researchers stated that ray tissue acting as stiffening ribs in the R direction contributed to lower compliance comparison with that for the T specimen [3, 4]. Meanwhile, the cellulose microfibrils are distorted by pits in the L direction giving the radial cell wall lower compliance [3]. Moreover, the irregular

polygonal cell structure in softwood might make the tangential compliance higher [25, 26].

The right panel of Fig. 4 demonstrates the master curve that takes 30 °C as the reference temperature and shifts the raw data curves at other temperatures horizontally along the $\log t$ axis to the 30 °C curve for each specimen. Thus, from a family of raw data curves at different temperatures, an overlapped master curve was generated for each specimen providing creep compliance values for an extended time period at the reference temperature. The extended time scale of master curves was dependent on grain orientation: the extended time for R and T specimens was similar, obviously longer than that for L specimen (Fig. 4). The creep time extrapolated to about 10^4 , 10^6 , and 10^6 s from 20 min isothermal creep test in this study for L, R, and T specimens, respectively. Furthermore, the overlapping curves of R and T specimens were quite well matched than that of the L specimen.

The horizontal shift factor recorded the horizontal movement for each creep segment and represented the ratio of relaxation times relative to those at the reference temperature (i.e., the shift factor required to transpose the temperature effect to the corresponding time effect). Figure 5 illustrates the horizontal shift factor values of 13 creep curves (30–150 °C) determined in all orthotropic directions, and the increased trend in the magnitude of the horizontal shift factor with elevating temperature was also found. The negative values of the horizontal shift factor indicated that the time needed for a given deformation was reduced and the creep was accelerated at higher temperature.

By fitting the horizontal shift factor data into the WLF equation and Arrhenius law, the solid line and dotted curve were plotted as shown in Fig. 5. Compared to the Arrhenius law, the WLF equation provided a better fitting with the horizontal shift factor over the entire temperature range in all orthotropic directions. The deviation from Arrhenius behavior indicated that a different type of dissipative mechanism occurred during the experiment. In general, standard error values can be used to evaluate the performance of model fitting. Based on Ferry [27], a successful fit result was obtained when the standard error value was less than 20. Table 1 presents the values of C_1 and C_2 of the WLF equation based on the horizontal shift factor, as well as the standard error and activation energy calculated from the two mathematical models, respectively. According to the values of standard error, only the excellent fit of the horizontal shift factor to the WLF equation (standard error of estimate < 9.19) was observed under the test condition. The values of activation energy determined by Arrhenius law were lower than those calculated by the WLF equation. This result was in agreement with the earlier study [14].

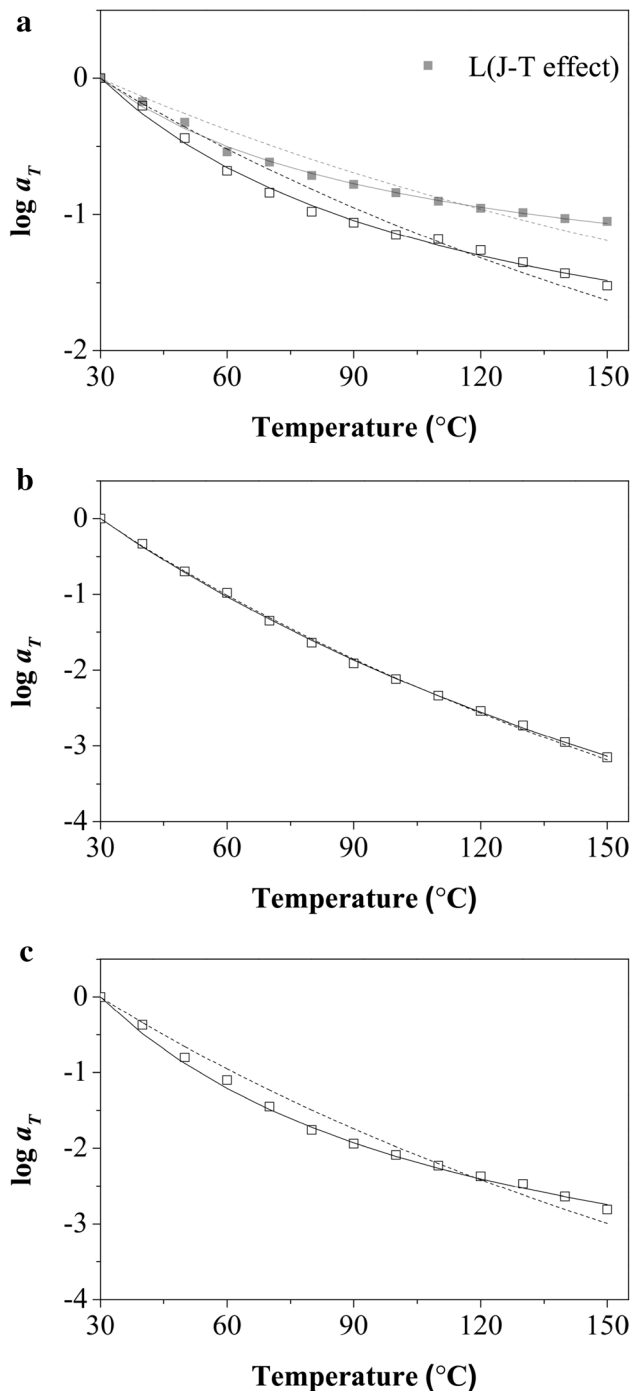


Fig. 5 Horizontal shift factor a_T (symbols) used to construct master curves at reference temperature 30 °C for the L (a), R (b), and T (c) specimens, and fit of the horizontal shift factor variation to the WLF equation (solid line) and Arrhenius law (dotted line). L (J - T effect) in a experimental data corrected by the vertical factor b_T for L specimen

The horizontal shift factor plots between R and T specimens were relatively similar, while the L specimen presented lower absolute value, as shown in Fig. 5. Moreover, the slope of the horizontal shift factor plots in

proportion to the activation energy was also different among the L, R, and T specimens. The activation energy associates with a mechanism of internal friction, which is defined as the difference in the energy between the atoms or molecules in an activated configuration, and the corresponding atoms or molecules in their initial configurations [14]. The activation energy values for L, R, and T specimens are presented in Table 1. According to the WLF equation, the values of activation energy for L, R, and T specimens were 12.36, 16.21, and 22.80 kcal mole⁻¹, respectively. Gamalath [28] reported that the activation energy of wood was 16.77–33.77 kcal mole⁻¹. Bond et al. [29] stated that the activation energy of Douglas fir (*Pseudotsuga menziesii*) at 9% moisture content was 15.5 kcal mole⁻¹ in tension parallel to the grain. The lower activation energy in the L specimen may be attributed to the stress modes, reference temperature, moisture content, and grain orientation. In general, the activation energy increased with increasing creep compliance because, as creep increased, greater distortions of bond angles and chain rotations occurred and a larger amount of energy was dissipated, resulting in a higher activation energy [3, 14]. This general trend was in agreement with the largest creep compliance and most activation energy obtained for the T specimen in this study and was confirmed by Placet et al. [14] as well.

Examination of experimental data in the ACP

To build a visual assessment of the master curve, the ACP was applied in all directions (Fig. 6). For R and T specimens, a continuously linear approximation consisted of the individual creep curves observed in the ACP. However, the ACP showed that the final overlapping was poor for the L specimen, and the same slope but different intercept of the trajectory with the J' -axis was found for individual creep curves. The structural arrangement of the wood cell wall can be viewed as a fiber composite system by cellulose microfibrils and hemicellulose–lignin matrix [24, 30]. In tensile tests, highly crystalline cellulose microfibrils dominated the creep behavior of the L specimen, while amorphous hemicellulose–lignin matrix was more pronounced for the R and T specimens [30–32]. When tensile stress was applied to the L specimen, the external stress induced specific molecular deformations of the cellulose microfibrils. The reorientation of cellulose microfibrils and the stretching of the C–O–C bridge between two glucose molecules in a cellulose microfibril caused the cellulose microfibrils to be regularly aggregated toward the cell axis. More importantly, temperature could aggravate the specific molecular deformations of the cellulose microfibrils (i.e., the oriented aggregation), resulting in temperature-dependent compliance (denoted here as the J - T effect)

Table 1 Parameters of the WLF equation and Arrhenius law for Chinese fir wood in all orthotropic directions

Specimens	WLF				Arrhenius	
	C_1	C_2 (K)	ΔH (kcal mole ⁻¹)	SE (%)	ΔH (kcal mole ⁻¹)	SE (%)
L	2.56	87.32	12.36	9.19	8.26	32.86
R	9.75	253.15	16.21	7.34	15.80	23.05
T	4.74	87.55	22.80	8.64	14.96	35.86
L (J - T effect)	1.71	72.02	9.97	5.97	5.86	28.53

WLF, William–Landel–Ferry equation, enunciated by Williams et al. [10], is given by $\log a_T = -C_1(T - T_0)/[C_2 + (T - T_0)]$; C_1 and C_2 , two WLF constants; ΔH , activation energy deduced from horizontal shift factor plots of raw experimental data; SE, standard error of the estimate; L (J - T effect), experimental data corrected by the vertical factor b_T for L specimen

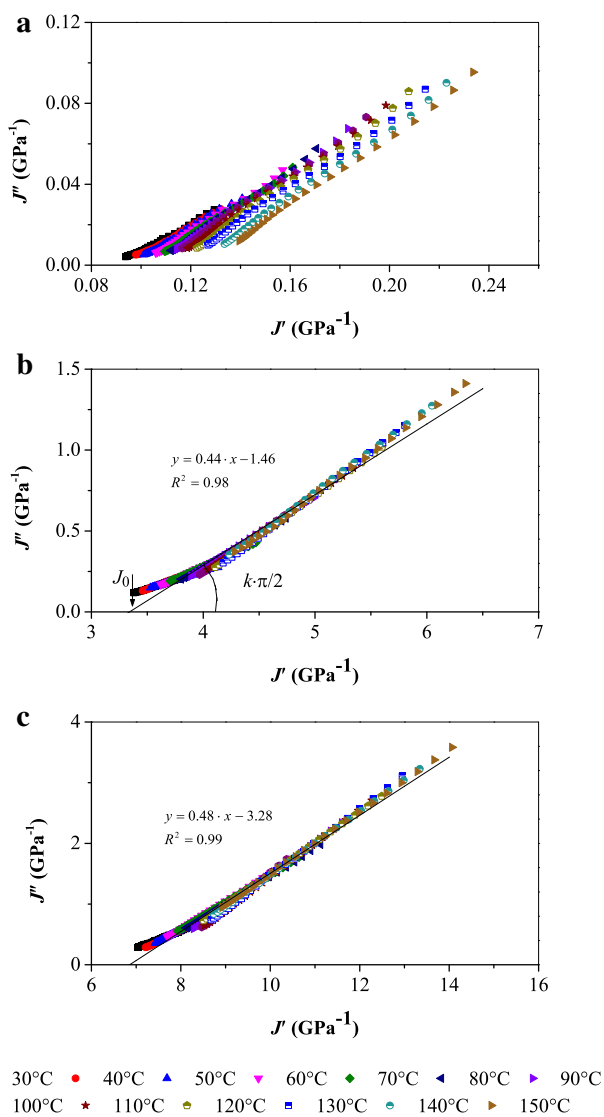


Fig. 6 Representation of the results in the approximated complex plane (ACP) for the L (a), R (b), and T (c) specimens based on Fig. 4. J' and J'' Alfrey's approximations of storage and loss compliance, respectively (Eqs. 4, 5); J_0 initial compliance; k power exponent

[24, 33–35]. According to some researches [12, 13, 36, 37], TTSP was applicable to amorphous polymers. The regularly oriented aggregation of highly crystalline cellulose microfibrils with the elevating temperature might result in an additional burden for the application of TTSP. Landel and Nielsen [36] suggested that the TTSP could be applied to most polymers, as long as a vertical shift factor, which was strongly dependent on temperature, was employed. A vertical shift factor b_T was introduced in this study accounting for the J - T effect [38], and the corrected compliance $J(t)_b$ was written as Eq. (6):

$$J(t)_b = J(t)/b_T, \tag{6}$$

where $J(t)$ is the creep compliance.

Based on the J - T effect, a homothetic transformation of longitudinal creep curves in the ACP was performed to eliminate the influence of temperature on compliance. The vertical shift factor b_T was adjusted to obtain a continuous curve, taking 30 °C as the reference temperature. A linear approximation was observed for the transformed ACP (J''/b_T with respect to J'/b_T) in Fig. 7. Moreover, the

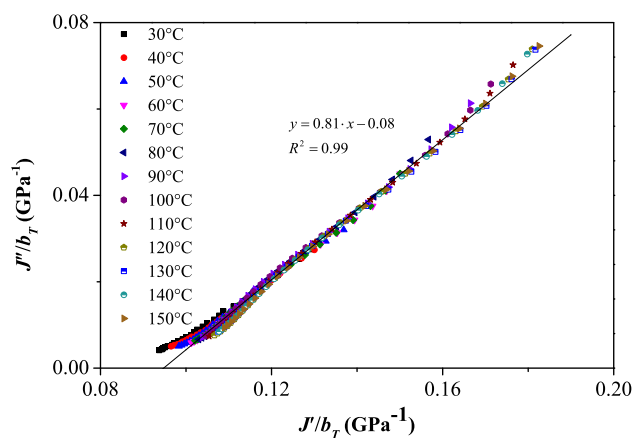


Fig. 7 ACP of the L specimen in Fig. 6 corrected by vertical factors b_T

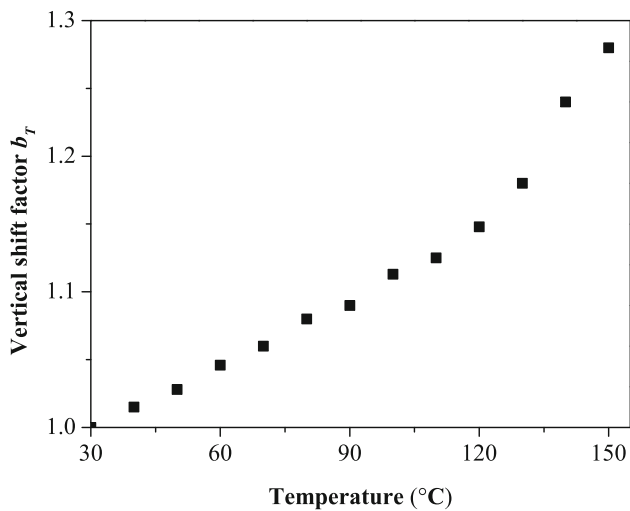


Fig. 8 Vertical shift factor b_T for the L specimen

temperature dependency of b_T (Fig. 8) showed an increasing trend in b_T with increasing temperature and the values of $b_T > 1$. The curve of vertical shift factor b_T versus temperature exhibited two different slopes, lower/higher than around 120 °C. The b_T increased sharply when the temperature was more than 120 °C. According to Back and Salmén [39], the glass transition of lignin occurred at a range between 130 and 205 °C for dry wood. Therefore, the deviation from the threshold temperature 120 °C was probably ascribed to the glass transition of lignin. The glass transition of lignin intensified the reorientation of cellulose microfibrils and caused the amount of increasing b_T to be aggravated above 120 °C.

The TTSP was applied as soon as the continuity between individual creep curves in the ACP was satisfied. The corrected longitudinal data by the J – T effect were used to construct a master curve; Fig. 9 depicts the

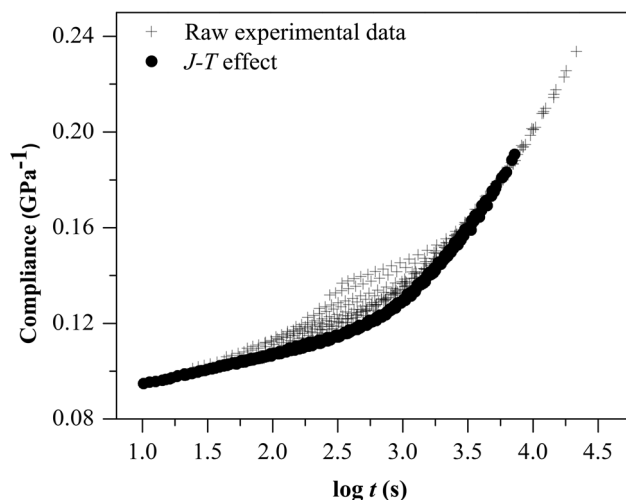


Fig. 9 The master curves of raw experimental data and corrected by the J – T effect for the L specimen

perfectly smooth master curve accounting for the J – T effect. Furthermore, the temperature dependency of the horizontal shift factor after correction is represented in Fig. 5a. The temperature dependency of the horizontal shift factor a_T plots for L specimen presented difference between raw data and data corrected by the J – T effect: after the J – T effect correction, a lower absolute value of a_T was found. The WLF equation provided a better fitting with the horizontal shift factor than Arrhenius law after correction (Fig. 5a), and the parameters of the two models are listed in Table 1. As compared to the activation energy of raw data for the L specimen, the J – T effect resulted in lower activation energy (Table 1). This indicated that considering the J – T effect would reduce the internal friction of wood cell wall by making the molecular chain flexible, and the distortions of bond angles and chain rotations became easier.

Creep model

Master curves were developed for Chinese fir in tension using short-term creep tests for the L, R, and T specimens. Power law equations were then applied for each master curve using a nonlinear fitting procedure. Based on the approximately straight line of experimental data in the (transformed) ACP (Figs. 6 “R”, “T”, 7), the power law model was derived as in Eq. (7):

$$J(t) = J_0[1 + a \cdot t^k], \tag{7}$$

where J_0 is the initial compliance, k the kinetic parameter and a the estimated parameter. The model parameters J_0 and k were directly identified from the ACP (Figs. 6 “R”, “T”, 7) and presented with a in Table 2.

The creep model showed very good agreement between modeled and master curves for each specimen, as illustrated in Fig. 10. The variation of initial compliance J_0 among the L, R, and T specimens (Table 2) also confirmed the aforementioned orthotropic compliance. According to Douhá et al. [8], the kinetic parameter k of five tropical species likely related to structural diversity, but the link between them was not clear. In this study, the creep model parameters also showed variation with grain orientation for Chinese fir. This opened expectations on future work

Table 2 Power law model parameters for Chinese fir wood in all orthotropic directions

Specimens	J_0 (GPa ⁻¹)	k	$a \times 10^{-3}$ (s ⁻¹)	RMS error (%)
L	0.09	0.51	11.17	0.00
R	3.33	0.28	1.99	0.00
T	6.85	0.30	2.12	0.01

J_0 , initial compliance; k and a , power law parameters; RMS error, root mean square error between modeled and measured compliance values

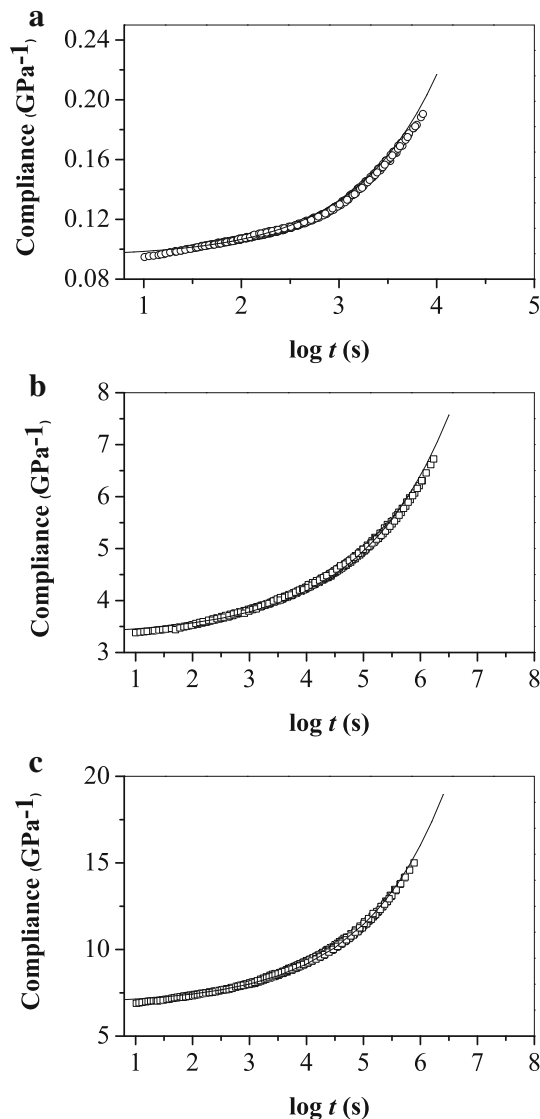


Fig. 10 Agreement between master curves (*symbols*) and power law model (*solid line curves*) determined for the L (a), R (b), and T (c) specimens

relying on the understanding of the physical meaning of the model parameters.

Conclusions

The validation of TTSP was a vital task prior to the practical application. In this study, a sequence of short-term creep tests for dry wood at 10 °C interval in the temperature range of 30–150 °C was conducted in the L, R, and T directions. The main conclusions are as follows:

- Creep compliance was dependent on temperature and orthotropic directions. Creep was accelerated with

elevating temperature, resulting in reducing the time required for a given deformation.

- The overlapping curves of the R and T specimens were quite well matched than the L specimen for dry wood only using horizontal shift factor over the temperature range of 30–150 °C. However, the compliance curve for the L specimen required an additional vertical shift factor to construct a smooth master curve because of the effect of temperature on longitudinal compliance.
- The creep model governed by a power law depicted the master curve for each specimen and showed the relevance between the model parameters and ACP data.
- Finally, the present work partially fills up the applicability of TTSP to wood rheological properties and provides the firsthand data on the anisotropic TTSP's applicability. In addition, the work successfully builds the rheological model in three grain directions to predict the orthotropic creep response.

Acknowledgements This research was sponsored by the National Natural Science Foundation of China (31570548).

References

1. Miyoshi Y, Furuta Y (2016) Rheological consideration in fracture of wood in lateral tension. *J Wood Sci* 62:138–145
2. Kaboorani A, Blanchet P, Laghdir A (2013) A rapid method to assess viscoelastic and mechanosorptive creep in wood. *Wood Fiber Sci* 45:370–382
3. Forest Products Laboratory (1987) *Wood handbook*. Agriculture handbook, vol 72. USDA Forest Service, Washington, DC
4. Bodig J, Jayne BA (1982) *Mechanics of wood and wood composites*. Von Nostrand Reinhold Company, New York
5. Navi P, Stanzl-Tschegg S (2009) Micromechanics of creep and relaxation of wood. A review COST Action E35 2004–2008: wood machining—micromechanics and fracture. *Holzforchung* 63:186–195
6. Chang FC, Lam F, Kadla JF (2013) Using master curves based on time-temperature superposition principle to predict creep strains of wood-plastic composites. *Wood Sci Technol* 47:571–584
7. Ma X, Jiang Z, Tong L, Wang G, Cheng H (2015) Development of creep models for glued laminated bamboo using the time-temperature superposition principle. *Wood Fiber Sci* 47:141–146
8. Dlouhá J, Clair B, Arnould O, Horáček P, Gril J (2009) On the time-temperature equivalency in green wood: characterisation of viscoelastic properties in longitudinal direction. *Holzforchung* 63:327–333
9. Wang F, Huang T, Shao Z (2017) Application of TTSP to wood-development of a vertical shift factor. *Holzforchung* 71:51–55
10. Williams ML, Landel RF, Ferry JD (1955) The temperature dependence of relaxation mechanisms in amorphous polymers and other glass-forming liquids. *J Am Chem Soc* 77:3701–3705
11. Goodrich T, Nawaz N, Feih S, Lattimer BY, Mouritz AP (2010) High-temperature mechanical properties and thermal recovery of balsa wood. *J Wood Sci* 56:437–443
12. Kelley SS, Rials TG, Glasser WG (1987) Relaxation behaviour of the amorphous components of wood. *J Mater Sci* 22:617–624
13. Laborie MPG, Salmén L (2004) Cooperativity analysis of the in situ lignin glass transition. *Holzforchung* 58:129–133

14. Placet V, Passard J, Perré P (2007) Viscoelastic properties of green wood across the grain measured by harmonic tests in the range 0–95°C: hardwood vs. softwood and normal wood vs. reaction wood. *Holzforschung* 61:548–557
15. Sun N, Frazier CE (2007) Time/temperature equivalence in the dry wood creep response. *Holzforschung* 61:702–706
16. Taniguchi Y, Ando K, Yamamoto H (2010) Determination of three-dimensional viscoelastic compliance in wood by tensile creep test. *J Wood Sci* 56:82–84
17. Ando K, Mizutani M, Taniguchi Y, Yamamoto H (2013) Time dependence of Poisson's effect in wood III: asymmetry of three-dimensional viscoelastic compliance matrix of Japanese cypress. *J Wood Sci* 59:290–298
18. Kawahara K, Ando K, Taniguchi Y (2015) Time dependence of Poisson's effect in wood IV: influence of grain angle. *J Wood Sci* 61:372–383
19. Dastoorian F, Tajvidi M, Ebrahimi G (2010) Evaluation of time dependent behavior of a wood flour/high density polyethylene composite. *J Reinf Plast Compos* 29:132–143
20. Alfrey T (1948) *Mechanical behavior of high polymers*. Interscience, New York
21. Larsen F, Ormarsson S (2014) Experimental and finite element study of the effect of temperature and moisture on the tangential tensile strength and fracture behavior in timber logs. *Holz-forschung* 68:133–140
22. Backman AC, Lindberg KAH (2001) Differences in wood material responses for radial and tangential direction as measured by dynamic mechanical thermal analysis. *J Mater Sci* 36:3777–3783
23. Bader TK, Hofstetter K, Eberhardsteiner JA, Keunecke D (2012) Microstructure–stiffness relationships of common yew and Norway spruce. *Strain* 48:306–316
24. Salmén L, Burgert I (2009) Cell wall features with regard to mechanical performance. A review COST Action E35 2004–2008: wood machining–micromechanics and fracture. *Holzforschung* 63:121–129
25. Kifetew G (1999) The influence of the geometrical distribution of cell-wall tissues on the transverse anisotropic dimensional changes of softwood. *Holzforschung* 53:347–349
26. Mishnaevsky L, Qing H (2008) Micromechanical modelling of mechanical behaviour and strength of wood: state-of-the-art review. *Comput Mater Sci* 44:363–370
27. Ferry JD (1980) *Viscoelastic properties of polymers*. Wiley, New York
28. Gamalath SS (1991) Long term creep modeling of wood using time temperature superposition principle. Dissertation, Virginia Polytechnic Institute and State University, Blacksburg, VA
29. Bond BH, Loferski J, Tissaoui J, Holzer S (1997) Development of tension and compression creep models for wood using the time-temperature superposition principle. *For Prod J* 47:97–103
30. Englund ET, Svensson S (2011) Modelling time-dependent mechanical behaviour of softwood using deformation kinetics. *Holzforschung* 65:231–237
31. Bergander A, Salmén L (2002) Cell wall properties and their effects on the mechanical properties of fibers. *J Mater Sci* 37:151–156
32. Salmén L (2004) Micromechanical understanding of the cell-wall structure. *C R Biol* 327:873–880
33. Gierlinger N, Schwanninger M, Reinecke A, Burgert I (2006) Molecular changes during tensile deformation of single wood fibers followed by Raman microscopy. *Biomacromol* 7:2077–2081
34. Salmén L (2006) Ultra-structural arrangement and rearrangement of the cellulose aggregates within the secondary cell wall. Proceedings of the Fifth Plant Biomechanics Conference. STFI-Packforsk, Stockholm, pp 215–220
35. Kamiyama T, Suzuki H, Sugiyama J (2005) Studies of the structural change during deformation in *Cryptomeria japonica* by time-resolved synchrotron small-angle X-ray scattering. *J Struct Biol* 151:1–11
36. Landel RF, Nielsen LE (1993) *Mechanical properties of polymers and composites*. CRC Press, New York
37. Tajvidi M, Falk RH, Hermanson JC (2005) Time–temperature superposition principle applied to a kenaf-fiber/high-density polyethylene composite. *J Appl Polym Sci* 97:1995–2004
38. Maiti A (2016) A geometry-based approach to determining time-temperature superposition shifts in aging experiments. *Rheol Acta* 55:83–90
39. Back EL, Salmén NL (1982) Glass transition of wood components hold implications for molding and pulping processes. *Tappi J* 65:107–110